



Three-Dimensional Static and Dynamic Analyses of an Asphalt-Concrete Core Dam

Yingli Wu^{1,2}(✉), Xinwen Jiang³, Hua Fu^{1,2}, Kai Xu^{1,2},
and Zhiqiang Wu^{1,2}

¹ Nanjing Hydraulic Research Institute, Nanjing 210024, China
wuyingli@nhri.cn

² State Key Lab of Hydrology-Water Resources and Hydraulic Engineering,
Nanjing 210024, China

³ Gil Ziegler Hydro-project Construction Administration Bureau of Sikeshu
River, Wusu City, Xinjiang 833300, China

Abstract. The three-dimensional finite element method is employed to study the static and dynamic behavior of an asphalt-concrete core rockfill dam. The results show that the distribution of the stress and deformation of the asphalt-concrete core at the completion stage and during the operating period is reasonable and the core won't experience shear failure. Second, the vertical stress within the impervious core is higher than the upstream hydrostatic pressure, and hydraulic fracture is thought to be impossible. Third, under earthquake loading, an obvious whipping effect can be seen at the crest of the dam. The higher the input earthquake acceleration peak is, the larger the value of the maximum acceleration response of the dam body will be. The distribution of the maximum dynamic displacement of the dam is similar to that of the maximum acceleration response. In addition, under earthquake loading, the shear strength of the asphalt-concrete core is higher than the shear stress of the core, meaning that shear failure will neither occur in the core under dynamic loading. Through the systemic research on the static and dynamic behavior of the asphalt-concrete core dam, it can be obtained that the impervious system of the dam is good at the completion and impounding stages and the stress and the deformation behaviors of the dam are also good under earthquake loading. The results also show that better joining forms of the dam core and the impervious wall are put forward through optimization design to improve the stress deformation at this part and guarantee the safety of the dam body.

Keywords: Asphalt-concrete core dam · Static and dynamic computing
Three-dimensional finite element · Dynamic response · Safety evaluation

1 Introduction

With the development of construction techniques, the advantage of using an asphalt concrete as the core material for rockfill dams is becoming more and more obvious and a dam with an asphalt-concrete core has become a very competitive choice. Up to now,

The National Key Research and Development Program of China (Grant No. 2017YFC0404800).

© Springer Nature Singapore Pte Ltd. 2018

A. Zhou et al. (Eds.): GSIC 2018, *Proceedings of GeoShanghai 2018*

International Conference: Fundamentals of Soil Behaviours, pp. 583–593, 2018.

https://doi.org/10.1007/978-981-13-0125-4_65

the world has a history of nearly 50 years to use the asphalt concrete as the interior impervious material for dams and has attained much valuable experience in design and construction. In western China, geological conditions are very complicated and earthquakes happen frequently. Unfortunately, many dams are located in such high seismic zones [1, 2]. As there are rare reports about dams with an asphalt-concrete core that have ever experienced earthquakes, their seismic responses are not very clear. Numerical simulation may shed some useful light on this topic [3].

Compared with concrete face rockfill dams, asphalt-concrete core dams are still in the stage of development and practical experience in building this kind of dams is relatively not rich [4]. According to the characteristics of asphalt-concrete core dams, scholars at home and abroad have done some researches about it [5–12]. In this paper, a three-dimensional finite element model was developed for an asphalt-concrete core dam located on a deep overburden layer in the north-west of China. In particular, Duncan and Chang's nonlinear constitutive model was used to study the performance during construction and impounding, and the equivalent viscous elastic dynamic model was employed to study its dynamic responses under earthquake loading. The stress and deformation characteristics of the dam body and its impervious system were analyzed. Finally, the seismic safety evaluation of the dam was performed, which provides scientific evidence for the seismic design of asphalt-concrete core dams.

2 Calculation Principles and Constitutive Models

In this paper, Duncan and Chang nonlinear constitutive model and the equivalent viscous elastic dynamic model were used to study the distribution regularity of stress and deformation characteristics of the dam body (for the stage of completion and impounding) respectively. And other results were also obtained from these two models, including the dynamic response acceleration, dynamic displacements and the distribution regularity of dynamic shear stress under earthquake loading.

2.1 Constitutive Models

Duncan and Chang nonlinear constitutive model was used to calculate the static. This model includes two variables: Young's tangent modulus E_t and tangent bulk modulus K_t . By the following equation, these two variables are calculated as

$$E_t = KP_a(\sigma_3/p_a)^n(1 - R_f S_t)^2 \quad (1)$$

$$K_t = K_b P_a(\sigma_3/p_a)^m \quad (2)$$

where P_a is atmospheric pressure; K is the coefficient of Young's modulus; n is the exponent determining the rate of variation of E_t with confining pressure σ_3 ; R_f is failure ratio; S_t is stress level, which can be expressed as

$$S_l = \frac{(\sigma_1 - \sigma_3)(1 - \sin\varphi)}{2c \cos\varphi + 2\sigma_3 \sin\varphi} \tag{3}$$

in which, c and φ are shear strength indexes.

The equivalent viscous elastic dynamic model was used to calculate the dynamic response. Dynamic shear modulus G and damping ratio λ can be calculated as

$$G = \frac{k_2}{1 + k_1 \gamma_d} P_a \left(\frac{\sigma_m}{P_a} \right)^{n'} \tag{4}$$

$$\lambda = \frac{k_1 \bar{\gamma}_d}{1 + k_1 \bar{\gamma}_d} \lambda_{max} \tag{5}$$

in which, $\sigma_m = (\sigma_1 + \sigma_2 + \sigma_3)/3$; γ_d is dynamic shear strain; k_1 and k_2 are constants of dynamic shear modulus; λ_{max} is the maximal damping ratio; $\bar{\gamma}_d$ is the normalized dynamic shear strain.

$$\bar{\gamma}_d = \gamma_d (\sigma_m / p_a)^{n'-1} \tag{6}$$

2.2 Computing Model

In the model, the maximum height of the dam is 102.5 m, the thickness and the length of the dam crest are 10 m and 345 m. The outer slopes of the dam are 1:2.0 upstream and 1:1.8 downstream. The vertical asphalt concrete core is 1.2 m wide and the concrete anti-seepage wall has 1-meter width. Three borrow areas provide the required material for the dam body: the blasting material zone, the transition zone and the sand and gravel zone. The bottom boundary of the model is the weakly-weathered layer. The boundaries of the cross sections of the upstream and downstream of the dam are assumed to be the same as the dam height. The boundary of the axis of the dam is assumed to be the bed rock of the river. Movement in the direction of the upstream and downstream sides and movement in the directions of bed rock in the bottom and on both sides of the river are restricted for the model. The interaction between the concrete anti-seepage wall and the overburden layer is modeled by applying an interface between them. The three-dimensional finite element mesh of dam body is shown in Fig. 1.

2.3 The Parameters of Static and Dynamic Analyses

In the static analyses of the concrete anti-seepage wall and the bedrock underlying the dam, the elastic material parameters were used. Duncan and Chang nonlinear constitutive model was used to study the deformation characteristics of the dam body and the overburden layer. The model parameters of different required materials for the dam body are shown in Tables 1 and 2 respectively. Then the equivalent viscous elastic dynamic model was employed in the dynamic analyses of the concrete anti-seepage wall and the bed rock in the dam bottom and the parameters are shown in Table 3.



Fig. 1. The three-dimensional finite element mesh of dam body.

Table 1. Elastic parameters of static analysis.

Material	Density (g/cm ³)	Elasticity modulus (GPa)	Poisson's ratio
Concrete anti-seepage wall (C35)	2.45	31.5	0.167
Weathered bedrock	2.70	2.97	0.3

Table 2. Parameters of static analysis.

Dam materials	Density (g/cm ³)	<i>c</i> (kPa)	ϕ_0 (°)	$\Delta\phi$ (°)	<i>K</i>	<i>n</i>	<i>R_f</i>	<i>k_b</i>	<i>m</i>
Asphalt concrete	2.43	400	27	0	850	0.33	0.76	2600	0.25
Transition	2.22	0	52.3	7.8	815	0.29	0.61	319	0.35
Rockfill of the shell	2.13	0	53.2	9.8	1006	0.28	0.63	477	0.17
Gravel sand of the shell	2.23	0	51.0	7.0	754	0.29	0.61	311	0.28
Overburden layer material I	2.06	0	51.0	7.6	509	0.59	0.73	350	0.20
Overburden layer material II	2.16	0	52.9	8.0	922	0.44	0.62	658	0.15
Overburden layer material III	2.26	0	55.1	8.9	1250	0.37	0.30	1004	0.11
Overburden layer material IV	2.20	0	54.2	8.7	1123	0.42	0.64	906	0.13

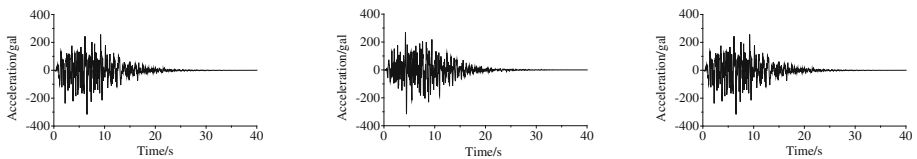
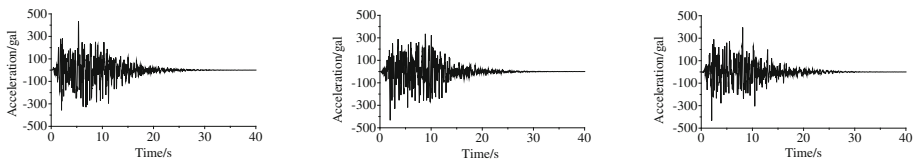
2.4 Seismic Wave

In the paper, the synthetic seismic wave was provided by China Earthquake Administration. 10-percent and 5-percent exceedance probability seismic waves over a 50-year recurrence interval from the dam site were selected to be used in the model. The peak ground accelerations are 253 gal and 346 gal respectively. The research of the dynamic response characteristics of the asphalt-concrete core was performed.

Table 3. Parameters of dynamic analysis.

Required materials for the dam	k_2	λ_{max}	k_1	n'
Asphalt concrete	1600	0.20	10.0	0.50
Rockfill of the shell	2441	0.21	17.2	0.27
Transition	2352	0.20	15.3	0.31
gravel sand of the shell	2096	0.21	24.8	0.37
Overburden layer material I	1864	0.23	26.0	0.43
Overburden layer material II	1936	0.23	25.5	0.44
Overburden layer material III	2361	0.21	22.5	0.26
Overburden layer material IV	2500	0.20	20.0	0.25

And the synthetic seismic waves were input from the bedrock. Figures 2 and 3 show the acceleration histories for 10-percent and 5-percent exceedance probability seismic waves over a 50-year recurrence interval.

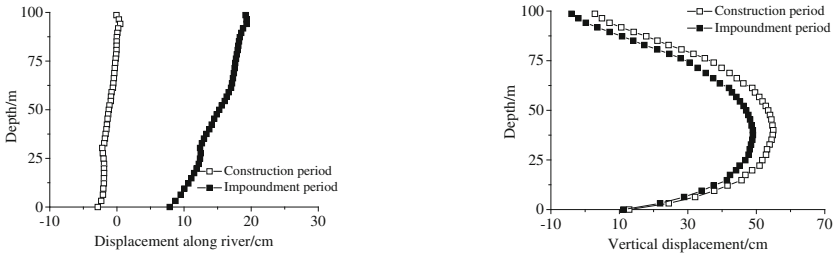
**Fig. 2.** Acceleration histories with 10% of the 50 years transcendental probability.**Fig. 3.** Acceleration histories with 5% of the 50 years transcendental probability.

3 Computing Results and Analyses

Systemic researches of the operating characteristics of the impervious system of the asphalt-concrete core were performed under static and dynamic loads. Results show the stress deformation characteristics of the asphalt-concrete core and the anti-seepage wall. In the Fig. 4, the stress is positive in compression. And the displacements towards the downstream of the river and the downward vertical displacements are assumed to be positive.

3.1 Seismic Wave

The Displacements of the Dam Core. Figure 4 presents the distribution curves of the horizontal displacements towards the downstream and the vertical displacements of the dam core cross section at the stage of completion and impounding. The bottom of the dam core is set to be the origin of the coordinate.



(a) The horizontal displacement of the core (b) The vertical settlement of the core

Fig. 4. The regularity of distribution of the dam core deformation characteristics.

Figure 4(a) shows the horizontal displacement towards the downstream occurs in the dam core due to the stiffness differences between the two parts of the dam body on the upstream and downstream sides after the end of construction. And during this period, the value of the horizontal displacement is very small. After impounding, the upstream hydrostatic pressure causes the occurrence of the horizontal displacements towards the downstream in the dam core. In addition, Fig. 4(a) shows the maximal horizontal displacement occurs at the top of the dam core and the amount of the maximum displacement is 19 cm. Figure 4(b) presents the distribution curve of the dam core settlement. The maximum settlement occurs at the position of 1/3 the height of the dam. And the maximum settlement is 55 cm. Without considering the deformation of sand and gravel during impounding, the maximum settlement decreases slightly under the hydrostatic pressure and the amount of the maximum settlement is 49 cm during impounding.

The Stress State of the Dam Core During Impounding. Figure 5 shows the contours of major principal stress, minor principal stress and stress level during impounding. The maximum values of major principal stress and minor principal stress are 1200 kPa and 700 kPa. During impounding, the dam core is under the compressive stress. Due to the effect of the river valley on the two sides of dam core, the minor principal stress decreases near the intersection of the dam core and the bank slope, which is the obvious effect of stress arch. The stress level during impounding isn't very high. And the maximum stress is 0.6, which occurs at the junction between the bottom of the dam core and the anti-seepage wall. It shows that the shear stress is much lower than the shear strength during the operating period and the stress state of the core is good.

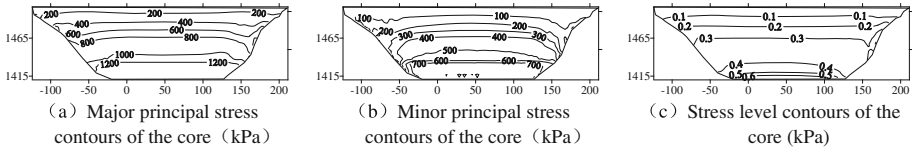


Fig. 5. The stress contours of the asphalt-concrete core.

The Hydraulic Fracture of the Dam Core. The hydraulic fracture of the dam core is an important concern in the construction and operation of the dam. The method of comparing the vertical stress of the dam core and the hydrostatic pressure acting on the core was employed to judge whether the hydraulic fracture will occur. Figure 6 shows after impounding, the vertical stress of the dam core is much higher than the hydrostatic pressure caused by impounding. The closer it gets to the bottom of dam, the larger the ratio of the vertical stress of the dam core to the hydrostatic pressure will be, which shows that the vertical stress of the dam core is higher than the hydrostatic pressure, so the hydraulic fracture won't occur.

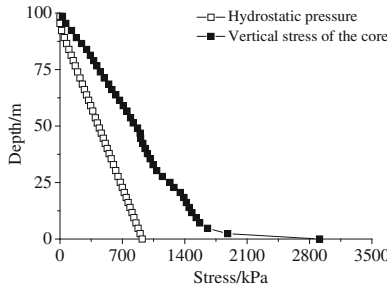


Fig. 6. Hydraulic fracturing analysis of core

3.2 Dynamic Computing Results and Analyses

The researches of the dynamic response characteristics, the seismic behavior and the dynamic operating characteristics of the asphalt-concrete core dam under different input combinations of seismic waves were performed, which provides reference for the seismic design of the dam.

The Dynamic Response of the Dam Body. Figure 7 shows the contours of the horizontal acceleration amplification towards the downstream and the vertical acceleration amplification of the maximum dam cross section for different exceedance probabilities of seismic waves. The maximum horizontal acceleration amplification towards the downstream and vertical acceleration amplification for 10% exceedance probability seismic wave are 2.80 and 2.41 respectively. What's more, the maximum horizontal acceleration amplification towards the downstream and vertical acceleration amplification for 5% exceedance probability seismic wave are 2.42 and 2.23

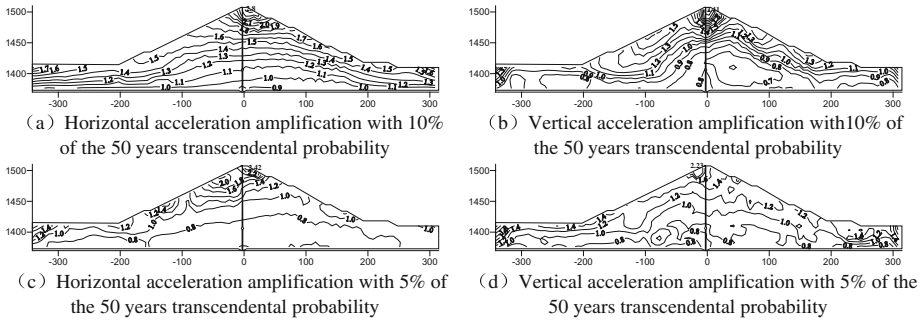


Fig. 7. The dynamic response acceleration amplification of the maximum dam cross section.

respectively. It can be shown that the higher the earthquake peak acceleration is, the more violent the dam acceleration response will be and the lower the response acceleration amplification of the dam will be. The dam acceleration response law under earthquake loading is consistent with the ordinary dam response law. The maximum acceleration response occurs at the dam crest, which is the obvious whipping effect.

The maximum horizontal displacement towards the downstream and vertical dynamic displacement of the dam for different exceedance probability seismic waves are shown in Fig. 7. The maximum horizontal displacement towards the downstream and vertical displacement under 10% exceedance probability seismic wave are 20 cm and 3.8 cm respectively. And the maximum horizontal displacement towards the downstream and vertical displacement under 5% exceedance probability seismic wave are 33 cm and 6 cm respectively. In addition, it can also be seen in the Fig. 8 that the maximum dynamic displacement decreases with the decrease of the height of the dam and the maximum dynamic displacement occurs at the dam crest.

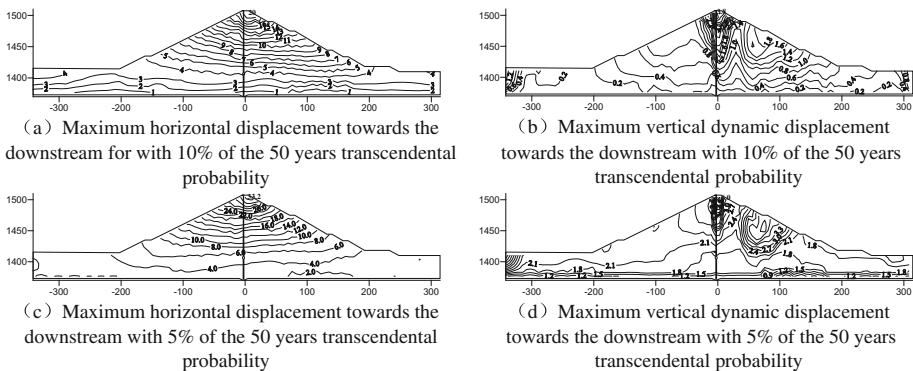


Fig. 8. The maximum dynamic displacement contours of the maximum dam cross section (cm).

The Dynamic Response of the Asphalt-Concrete Core. The dynamic shear stress peak contours of the asphalt-concrete core for 10% and 5% exceedance probability seismic waves were shown in the Fig. 9. The dynamic shear stress during impounding decreases with the increase of the height of the dam and the dynamic shear stress of the riverbed is larger than that on the two sides of the river. The dynamic shear stresses for the two kinds of exceedance probability seismic waves are 180 kPa and 330 kPa respectively.

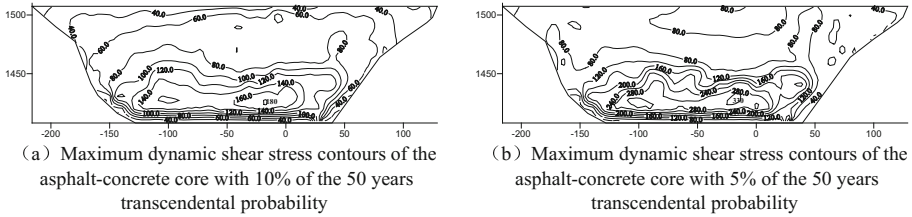


Fig. 9. The maximum dynamic shear stress contours of the asphalt-concrete core under earthquake loading (kPa).

Based on the Mohr-Coulomb model, the safety factor F_S is defined as the ratio of the unit shear strength to the unit shear stress. Then the shear safety factor contours of the vertical section of the asphalt-concrete core can be obtained in Fig. 10. It is shown from the results that the shear safety factor increases with the increase of the height of the dam. The maximum and minimum safety factor occurs at the dam crest and bottom respectively. The minimum safety factors at the dam bottom for 10% and 5% exceedance probability seismic waves are 1.2 and 1.1 respectively.

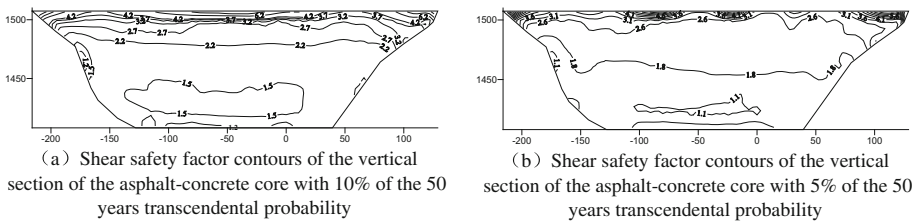


Fig. 10. The shear safety factor contours of the vertical section of the asphalt-concrete core under earthquake loading.

The Dynamic Response of the Concrete Anti-seepage Wall. The contours of the principal stress of the concrete anti-seepage wall during impounding overlaid by the maximum dynamic principal stress during earthquake loading were plotted in Fig. 11. After the static stress and the dynamic stress superimposed under 10% and 5% exceedance probability seismic waves, the maximum major principal stress occurs about 20 m below the middle anti-seepage wall. The maximum major principal stresses

in the two cases are 27.5 MPa and 28.0 MPa respectively. And the maximum minor principal stresses are 3.0 MPa and 5.0 MPa. Most parts of the anti-seepage wall are under the compressive stress and partial tensile stress only occurs near the intersection of the concrete anti-seepage wall and the bedrock on the two sides of the river. The tensile stresses are 4.6 MPa and 5.2 MPa. The concentrating is generated due to the boundary conditions, which leads to the distortion of the computing results.

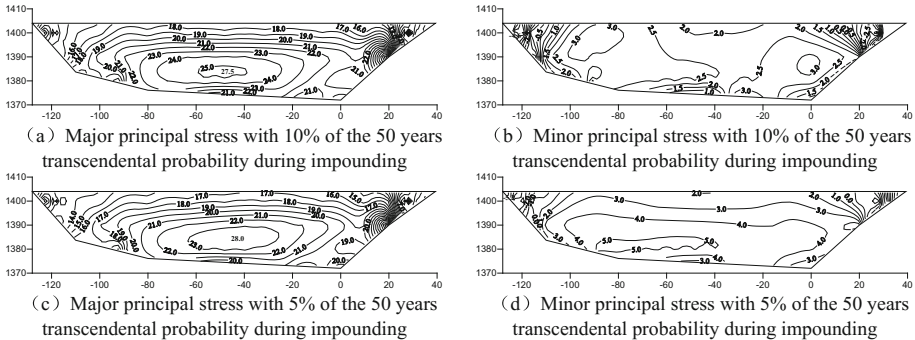


Fig. 11. The contours of the principal stress of the concrete anti-seepage wall during impounding overlaid by the maximum dynamic principal stress during earthquake loading (MPa)

4 Conclusions

- (1) The distribution of stress and deformation of the asphalt-concrete core at the completion stage and during the operating period is reasonable. The compressive stress and the stress level of the asphalt-concrete core is not high, below the strength of the used material, indicating that shear failure is not likely to happen in the core. Furthermore, the vertical stress along the asphalt wall is always higher than the hydrostatic pressure, so that hydraulic fracture is neither considered possible.
- (2) Under earthquake loading, obvious whipping effect can be observed at the crest of the dam. The higher the input earthquake acceleration peak is, the larger the value of the maximum acceleration response of the dam body will be. Second, the distribution of the maximum dynamic displacement of the dam is similar to that of the maximum acceleration response. What's more, under earthquake loading, the shear strength of the asphalt-concrete core is higher than the shear stress of the core. The minimum of the shear safety factor is 1.1, indicating that shear failure won't occur in the core under dynamic loading.
- (3) Through the systemic research on the static and dynamic characteristics of the asphalt-concrete core dam, it can be obtained that the impervious system of the dam is effective at the completion and impounding stages and the stress and the deformation behaviors of the dam are also satisfactory under earthquake loading, which meets the demands of the structure and seismic design of dams.

- (4) Better joining forms of the dam core and the impervious wall are put forward through optimization design to improve the stress deformation at this part and guarantee the safety of the dam body.

References

1. Zhao, J.M., Chang, Y.P., Chen, N.: Significance and prospects about earthquake resistant studies of high earth-rockfill dams. *Word Earthq. Eng.* **20**(1), 95–100 (2004)
2. Sheng, Z.: 3-D seismic response analysis of rockfill dam with asphalt concrete core. *Rock Soil Mech.* **29**(11), 2933–2938 (2008)
3. Sheng, Z.: Earthquake-induced damage and aseismic safety of earth-rock dam. *Word Earthq. Eng.* **30**(6), 40–51 (2011)
4. Ze-Yan, Y., Jianping, Z., Jiang, G.C., et al.: Development of CFRD in China. *Water Power* **37**(2), 18–23 (2011)
5. Bingyin, Z., Li, Q., Xiong, Y., et al.: Numerical study on Maopingxi rockfill dam with asphalt concrete core in the Three Gorges Project. *J. Yangtze River Sci. Res. Inst.* **21**(2), 18–21 (2004)
6. Tongchun, L., Xiaoqing, L., Songyou, X.: Study on asphalt concrete core type and size of Yele rockfill dam. *J. Hohai Univ.* **28**(2), 109–112 (2000)
7. Feizi-Khankandi, S., Ghalandarzadeh, A., Mirghasemi, A.A., Hoeg, K., et al.: Seismic analysis of the Garmrood embankment dam with asphalt concrete core. *Soils Found.* **49**(2), 153–166 (2009)
8. Guo, C.: Discussion on stress characteristics of concrete diaphragm wall. *Water Power* **7**, 18–22 (1995)
9. Cui, J., Shen, Z.: Characteristics of earthquake induced permanent deformation of a high composite dam with asphalt concrete core wall. *Water Resour. Power* **28**(1), 73–77 (2010)
10. Yuan, G., Huolang, H.F.: Seismic response analysis of rockfill dam based on 3D multi-mechanism model. *J. Disaster Prev. Mitig. Eng.* **33**(4), 375–383 (2013)
11. Kong, X.J., Yu, Y., Zou, D.G., et al.: 3D FE static and dynamic analysis of rockfill dam with asphalt concrete core. *J. Dalian Univ. Technol.* **54**(2), 197–203 (2014)
12. Qi, C., Liu, X., Wu, J., et al.: Three-dimensional liquefaction analysis of core-wall rockfill dam under different intensity earthquakes. *J. Disaster Prev. Mitig.* **34**(2), 143–148 (2014)